crystals

MDPI

Review

Optical and Electrical Properties of Low-Dimensional Crystalline Materials: A Review

Jose Luis Pura [1,2]

[1] GdS-Optronlab, Física de la Materia Condensada, Universidad de Valladolid, Paseo de Belén 19, 47011 Valladolid, Spain; joseluis.pura@uva.es
[2] Instituto de Estructura de la Materia (IEM-CSIC), Consejo Superior de Investigaciones Científicas, Serrano 121, 28006 Madrid, Spain

Abstract: Low-dimensional materials have been revolutionary in both the technological and research fields over the last decades. Since the discovery of graphene in 2004, and thanks to the technological improvements in nanotechnology achieved during this last century, the number of low-dimensional materials under research and their potential applications have not stopped increasing. In this review, we present a comprehensive tour of the principal 2D and 1D materials that compose the current state of the art and also the technological applications derived from them. In both cases, the focus will be on their optical and electrical properties, as well as the potential applications on novel photonic, electronic, or optoelectronic devices. For 2D materials, we will focus on a brief review of graphene-like materials, giving more emphasis to graphene derivatives, hexagonal boron nitride, and transition metal dichalcogenides. Regarding 1D materials, we will aim at metallic and semiconductor nanowires. Nevertheless, interesting 2D and 1D materials are mentioned in each section. The topic will be introduced using the related origin of their unique capabilities as a common thread. At the same time, we will try to remark on the differences and similarities between both groups and their physical relationship.

Keywords: low dimensional materials; graphene; transition metal dichalcogenides; 2D materials; nanowires; 1D materials; electrical properties; optical properties

Citation: Pura, J.L. Optical and Electrical Properties of Low-Dimensional Crystalline Materials: A Review. *Crystals* **2023**, *13*, 108. https://doi.org/10.3390/cryst13010108

Academic Editor: Bo Chen

Received: 19 December 2022
Revised: 30 December 2022
Accepted: 1 January 2023
Published: 6 January 2023

1. Introduction

Low-dimensional materials have been revolutionary in both the technological and research fields during the last decades. The interest in low-dimensional materials grew exponentially following the development of nanotechnology in the 1980s, with great hope in their new physical properties and their potential applications. Later on, the discovery of graphene in the 2000s rekindled interest in these materials, with a special focus on two-dimensional (2D) systems, driving the discovery of other atomically thin-layered materials. The emerging physical properties of low-dimensional materials directly led to novel applications that range over many scientific fields with a broad range of applications, including devices such as transistors [1–3], solar cells [4–6], batteries [7–9], or lasers [10–12], but they can also present other functionalities such as controlling of air and water pollutants [13], sensors [14,15], drug delivery [16], or cancer treatments [17]. In this review, we aim to present a common framework that can understand the unique physical properties of low-dimensional materials, but also provide an overview of the current state-of-the-art focus on the most recent lines of investigation and technological applications.

The success of physics in explaining the underlying laws that guide our universe has been repeatedly demonstrated over the years. Regardless of the diversity of fields that can be found in physics, the methodologies can be organized in a first approximation by considering the number of elements of the system under study. If the system has a relatively small number of elements (electrons, atoms, photons, etc.) quantum mechanics will be the

suitable tool to achieve a good physical description in terms of eigenstates and operators. In contrast, when the system tends to involve a huge number of elements, an atomistical approximation will be impractical; however, at this point, classical mechanics become handy. In this last situation, the system can be treated as continuous. By doing so, this kind of problem could be tackled with the use of tools such as thermodynamics, mechanics, or statistical physics. Of course, the success of the description will depend on the difficulty of the specific problem under study and the suitability of the employed tools. However, the key point in both cases is the existence of a well-defined framework that allows us to ask specific questions, provide answers and deal with new challenges.

These two limiting approaches led us to an outstanding comprehension of nature, especially during the last century. However, in the overlapping region between these two limits, certain physical systems that present too many elements to directly use the quantum formalism exist; at the same time, this number is not high enough to safely assume a continuous behavior. This intermediate scenario is full of interesting novel phenomenologies that are already leading the development of new paradigms and technologies, and many more that still remain unexplored.

Usually, there is a direct relationship between the number of constituents of a system and its physical extension. A large number of elements typically results in a much bigger system in terms of space. This matter becomes particularly clear when the principal elements of the system are atoms. On the other hand, we have the fundamental particles associated with the relevant physical magnitudes: e.g., electrons for electrical conductivity, photons for optical properties, or phonons for thermal conductivity. Within this picture, we can define low-dimensional materials as systems with one or several spatial dimensions similar to or smaller than the associated wavelength of the involved particles, typically in the nanoscale regime. To be specific, when considering optical properties, the dimensions should be compared with the light wavelength. Conversely, when the electrical properties are under study, it is the electron wavelength and/or mean free path that should be comparable to the system dimensions.

If we begin with a three-dimensional (3D) bulk material, we can start by confining the particles in one of the three dimensions. Let us choose the z-axis for simplicity. The system will transition from having an effective infinite length in this direction to having a finite (and relatively small) thickness, and two free dimensions. By doing this, we have obtained a two-dimensional (2D) material. The paradigmatic example of this category is graphene; however, previously to graphene, we could find physical effects on the 2D scale, such as the quantum hall effect [18], or a broad line of research around quantum wells [19,20], which eventually became the base technology for most of the commercially available laser diodes nowadays. Following graphene, other similar materials have been explored [21], broadening the range of available physical properties for 2D materials.

If we proceed further from the 2D material and confine one of the remaining free dimensions, we will obtain a one-dimensional (1D) material. In this group, we can find nanowires (NWs) or nanorods, nanofibers and nanotubes. The properties of NWs are as varied as the materials used for their fabrication. We can find semiconductor [22,23] and metallic nanowires [24,25] with applications in fields such as electronics and photonics, or NWs presenting superconductivity [26] with applications in light detection, electronics or quantum information [27]. Nanofibers are mainly employed because of their capability of enhancing the mechanical properties of composite materials, but can also be used as filters or sensors, among others [28]. Regarding the nanotubes, even if the typical example is the carbon-based case, i.e., carbon nanotubes (CNTs) [29], other examples with great interest still exist, such as silicon nanotubes for energy storage [30,31], boron nitride nanotubes or BCN nanotubes [32–34] composed of different quantities of boron, carbon and nitrogen atoms. The applications range from materials science to energy storage and sensing.

In order to have a closed picture of the topic, we must mention the last step of the iteration, i.e., the zero-dimensional (0D) systems. By starting from a 1D system and constraining the last available degree of freedom, we could finally obtain a system confined

in all the spatial dimensions. Nanoparticles and quantum dots are great examples of 0D systems. However, despite their appealing properties and applications [35,36], this review will keep its focus on 1D and 2D materials.

This sequential procedure of reducing the dimensionality of a physical system offers the advantage of understanding the subsequent alterations of the physical properties on each step by knowing the previous one. Given the knowledge of the properties of the 3D bulk material, we can analyze any low-dimensional material step by step. The most direct change that appears when reducing the dimensionality is most likely the one that takes place in the density of states (DOS). The DOS, usually named D(E), is a function of energy and represents the number of available states per unit volume between the energies E and E + dE. The DOS dramatically depends on the system dimensionality [37–39]. Figure 1 shows a representation of systems with dimensions ranging from 3 to 0 (Top), together with a plot of the expected functional dependence of the DOS of such systems (Bottom). Similarly, the DOS is directly linked to the properties of the system because it is needed for the calculation of most of the basic physical magnitudes, such as the total energy or the thermal and electrical conductivities [40]. As shown in Figure 1, the dimensionality shapes the DOS, which translates into radically different properties of each type of material.

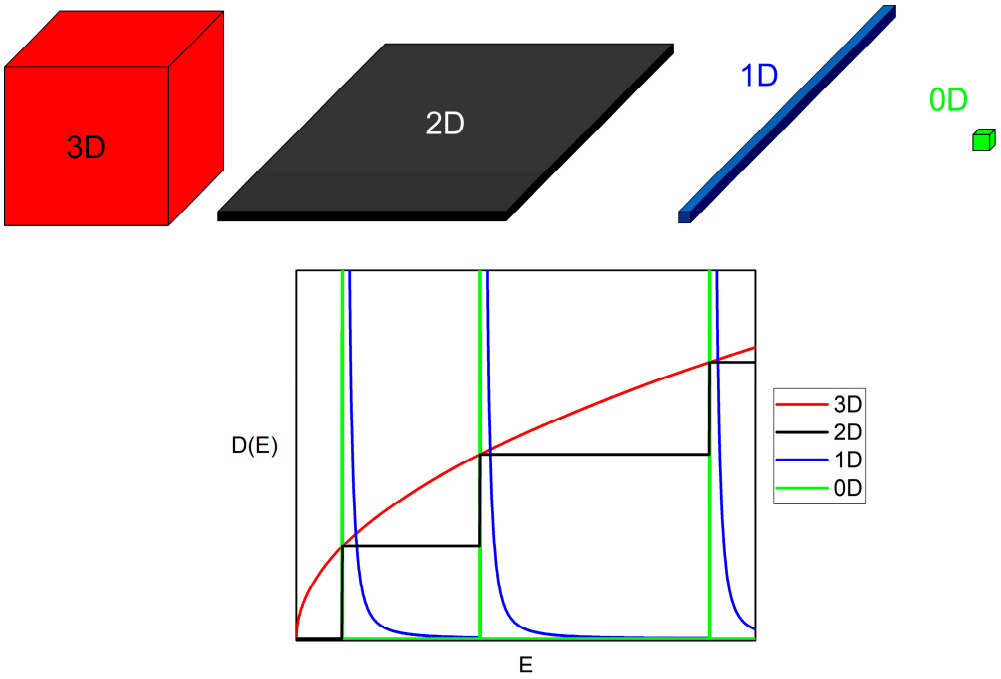

Figure 1. (**Top**) Schemes of bulk materials and the three possible low-dimensional materials derived from them. (**Bottom**) A plot of the functional dependence of the density of states (DOS) of each system.

Finally, the dependence of the physical properties on the dimensionality is important because it provides new capabilities to the studied materials far beyond those of the bulk materials. However, the key point of the properties–dimensionality relationship is the possibility of tailoring those properties by engineering the limiting dimensions.

2. 2D Materials

The aim of this section is to provide a review of the properties and applications of the most prominent 2D materials. The full group has been divided into three subgroups that cover most of the current scientific scenarios regarding electronic and optical applications.

Atomically thin 2D materials are characterized by their extremely low thickness. They are formed by a single layer of atoms connected by covalent bonds extending on the plane over distances much longer than its thickness. Despite the huge number of new materials

discovered in the last decade [21,41], we selected the most notable examples among the ones that have been proven to be stable. Table 1 presents a coarse organization in three different families of atomically thin 2D materials: graphene family, 2D chalcogenides, and 2D oxides.

Table 1. Overview of the different groups of atomically thin 2D materials. Adapted from Ref. [41] with updated information from Ref. [42] for 2D oxides. The graphene family includes carbon-based 2D materials, such as graphene and its derivatives, and hBN (known as "white graphene") and BCN. The 2D chalcogenides consist of all 2D compounds based on S, Se, and Te. The 2D Oxides gather those containing oxygen, excluding graphene oxide. The materials that have been proven to be stable in air and at room temperature are shaded in green. Those that could probably be stable under certain conditions given their similarities with the first group are shaded in yellow. Those that are known to be unstable in air but could be stable in certain inert atmospheres are shaded in orange/red. Finally, the grey-shaded compounds have been successfully obtained in the form of monolayers, which does not currently have much available information. "Others" indicates every other atomically thin crystal that could have been isolated or could be in the future.

<table>
<tr><th>Graphene Family</th><th>Graphene</th><th>hBN</th><th>BCN</th><th>Graphene Oxide</th><th>Fluorographene</th></tr>
<tr><td rowspan="2">2D Chalcogenides</td><td rowspan="2">MoS_2, WS_2, $MoSe_2$, WSe_2</td><td colspan="2" rowspan="2">Semiconducting dichalcogenides: $MoTe_2$, WTe_2, ZrS_2, $ZrSe_2$, etc.</td><td colspan="2">Metallic dichalcogenides: $NbSe_2$, NbS_2, TaS_2, TiS_2, $NiSe_2$, etc.</td></tr>
<tr><td colspan="2">Layered semiconductors: GaSe, GaTe, InSe, etc.</td></tr>
<tr><td rowspan="2">2D Oxides</td><td>Micas, BSCCO</td><td colspan="2">MoO_3, WO_3</td><td rowspan="2">Perovskite-type: $LaNb_2O_7$, $(Ca,Sr)_2Nb_3O_{10}$, $Bi_4Ti_3O_{12}$, $Ca_2Ta_2TiO_{10}$, etc.</td><td>Hydroxides: $Ni(OH)_2$, $Eu(OH)_2$, etc.</td></tr>
<tr><td>Layered Cu oxides</td><td>TiO_2, MnO_2, V_2O_5, TaO_3, RuO_2, etc.</td><td></td><td>Others</td></tr>
</table>

2.1. Graphene and Graphene Derivatives

The paradigmatic example of these materials is graphene [43,44]. It is formed by a hexagonal 2D arrangement of carbon atoms forming a honeycomb lattice, as seen in Figure 2. Intrinsic graphene behaves as a semimetal without a band gap. This implies that the motion of electrons in graphene obeys a Dirac-like equation. This distinctive behavior derived from its low dimensionality translates into exceptional physical properties such as ballistic transport of electrons, high electron mobility exceeding 15,000 $cm^2\ V^{-1}s^{-1}$ [45], high electrical and thermal conductivities, excellent optical transparency showing a 2.3% absorption of white light [46], or remarkable mechanical properties such as values of the Young modulus up to 300 N/m and the ability to sustain elastic deformations up to 15% [47]. Interestingly, when several monolayers of graphene are stacked under certain circumstances, their properties can change dramatically. This becomes especially fascinating when two layers of graphene are stacked together but are slightly rotated at a "magic angle" (~1.1°), and the result is known as twisted bilayer graphene (TBG). TBG has been shown to behave as an electric insulator [48], which contrasts with the good electric conductivity of single-layer graphene. TBG has also been shown to present superconductivity when electrostatic doping is present [49]. Further details about the properties of graphene can be found in the literature [50–52].

Regarding graphene derivatives, multiple possibilities for the obtention of these modifications of graphene exist [53]. Among the most relevant ones, we can find fluorographene and graphene oxide (GO). Fluorographene is a stoichiometric derivative of graphene that incorporates a fluorine atom bonded to each carbon atom [47,54]. It exhibits mechanical properties comparable to those of graphene, showing values of the Young modulus of 100 N/m and sustaining similar elastic deformations: ~15%. However, in contrast to graphene, fluorographene is an excellent electrical insulator, reaching resistivity values higher than 10^{12} Ω and presenting a band gap of ~3.0 eV [47]. It presents high stability in the air up to 400 °C and it is known as the 2D counterpart of Teflon.

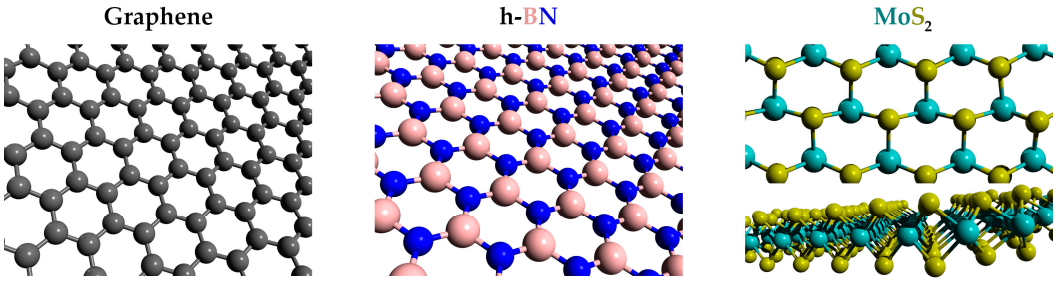

Figure 2. The crystalline structure of graphene, h-BN, and MoS_2 monolayers. The structure of other TMDs is the same as MoS_2.

GO is a non-stoichiometric modification of graphene that appears after its exposure to oxidizing agents. As a result, the pristine graphene sheets are modified by covalently attached oxygen groups such as hydroxyl, carboxyl, or epoxy groups. The surface of GO is typically inhomogeneous, showing pristine regions coexisting with zones with a high density of substituents [55,56]. The presence of oxygen-functional groups with covalent bonding gives GO outstanding mechanical properties [57,58]. Regarding the electrical response, GO is typically an insulator showing resistivity values higher than 10^{12} Ω [59], similar to fluorographene. However, GO can be synthesized by controlling the oxidation level to achieve semiconducting GO [60]. The possibility of controlling the chemical composition also permits the tunability of other optoelectronic properties [61,62]. The main advantage of GO is the high monolayer yield of the production process (>80%) [63]. This opened the path to obtaining large amounts of GO that can be then reduced to obtain reduced graphene oxide (rGO). Sadly, many properties of rGO do not match those of pristine graphene, especially the electrical conductivity. This appears as a consequence of the dramatic structural changes induced during the oxidation and subsequent reduction process, and the residual oxygen that cannot be removed. Nevertheless, great efforts are being made to bring rGO conductivity closer to that of graphene. Significant improvement has been obtained by the high-temperature annealing of rGO in the presence of a carbon source [64]. Given its properties, there is a great variety of applications for GO thin films in photovoltaics [65], photodetectors [66], transistors [62,67], transparent electric conductors [59,68,69], electrodes [70], or sensors [71–73].

2.2. Hexagonal Boron Nitride (h-BN)

Hexagonal boron nitride (h-BN) consists of a honeycomb array of boron and nitrogen atoms, as seen in Figure 2. The structure is analogous to that of graphene, but boron and nitrogen atoms occupy alternating positions in the 2D lattice maintaining a 1:1 relationship. As a result of its 2D nature, h-BN powder has been employed as an excellent lubricant. Regarding the electronic and optical properties, it is technically an insulator presenting a wide direct band gap of 6.07 eV [74]. According to this value, h-BN also presents light emission in the far ultraviolet region of the spectra. Its insulating behavior pairs with excellent dielectric properties: $\varepsilon \sim 3$–4 and a significantly high breakdown voltage (V_{break} = 0.7 V/nm) similar to that of SiO_2 (~1 V/nm) [75]. These interesting dielectric capabilities postulate hBN as the candidate to take the role of SiO_2 and other insulators in the manufacturing of graphene field effect transistors (GFETs). The use of hBN as a substrate of GFETs has been reported to improve carrier mobility up to 60,000 $cm^2/(Vs)$, three times higher than that achieved by using SiO_2 [76]. The improvement arises from the exceptionally low roughness of the hBN surface and the absence of surface charge traps and dangling bonds, which highly reduce carrier scattering. In addition, the reduced lattice mismatch between hBN and graphene helps to obtain an excellent interface between both 2D materials. In the same vein, Wang et al. designed a GFET based on a graphene monolayer sandwiched between hBN layers forming an hBN-graphene-hBN structure [77]. The hBN-based device is compared with an analogous SiO_2-graphene-Al_2O_3 FET demonstrating the mobility of the hBN-based GFET of 15,000 $cm^2\ V^{-1}s^{-1}$ (approximately eight times higher than its SiO_2/Al_2O_3 coun-

terpart), and a current-gain cut-off frequency (i.e., the frequency at which the current gain is equal to one) of 33 GHz (almost doubling the SiO_2/Al_2O_3 GFET performance).

Another application of hBN as a dielectric layer for FET improvement is provided by Lee et al. [78]. The use of hBN on a graphene/hBN/MoS_2 FET, as seen in Figure 3, showed an improvement of one order of magnitude in the mobility regarding the use of SiO_2, as well as the possibility of low gate voltage operation. Moreover, the inherent flexibility of all of the components allows its fabrication on a polymeric substrate demonstrating flexible and transparent devices with unchanged performance up to 1.5% strain.

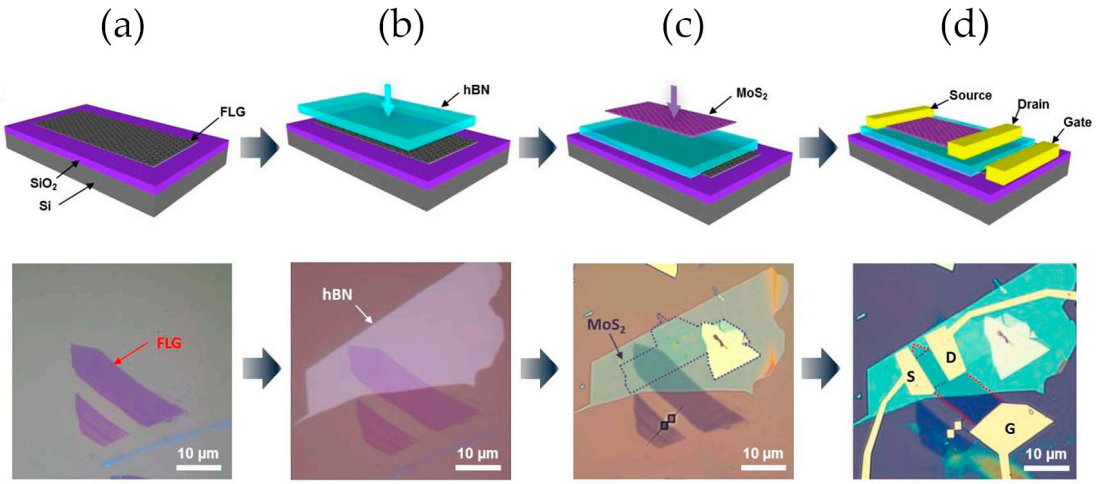

Figure 3. Schematic and optical images of the fabrication process of a graphene/hBN/MoS_2 FET. (**a**) Deposition of the few layers of graphene film. (**b**) Deposition of the hBN monolayer. (**c**) Deposition of the MoS_2 monolayer. (**d**) Fabrication of the metallic Au contacts. Reprinted (adapted) with permission from Ref. [78]. Copyright (2013) American Chemical Society.

2.3. Transition Metal Dichalcogenides (TMDs)

The 2D transition metal dichalcogenides (TMDs) are composed of a hexagonal 2D array of atoms of a certain transition metal element M, which is sandwiched between two hexagonal layers of chalcogen atoms X with structure X-M-X, as seen in Figure 2. Therefore, the transition metal (Mo, W, Nb, Ni, V, etc) combines with the chalcogen (S, Se, Te) following the stoichiometry MX_2. The combination of the first two metals and chalcogens in the lists, Mo, W, S, and Se, generate the top four most studied TMDs: MoS_2, WSe_2, $MoSe_2$, and WS_2 [79,80]. If all the possible combinations are considered, we end up with more than 40 different TMDs [81].

Depending on the combination of elements, TMDs can be obtained within different categories regarding their electrical conductivity. We find insulators such as HfS_2, semiconductors such as MoS_2, WSe_2, $MoSe_2$, and WS_2, semimetals such as $TiSe_2$, or metals such as NbS_2 and $NbSe_2$. Some of them, such as $NbSe_2$ or MoS_2, can even show superconductivity [82–84]. It is also possible to observe different electronic properties in one kind of TMD such as WTe_2, which has been shown to behave either as a superconductor [85] or as an insulator as a result of the quantum spin Hall effect [86]. Furthermore, the existence of excitonic insulating states has been recently observed [87].

The sustained interest over the last years in the group formed by MoS_2, WSe_2, $MoSe_2$, and WS_2 obeys three simple rules: they are relatively easy to obtain as monolayers compared to other TMDs, they are stable in air, and they present attractive values of the band gap within the visible range, as seen in Table 2 and Figure 4. Unlike their bulk counterparts [88] which present an indirect band gap in a much lower energy range, the direct visible band gap of the monolayers has an immediate impact on their optical properties. It has been shown that the photoluminescence (PL) of few-layer MoS_2 increases as the number of monolayers is reduced [89], and the maximum PL is achieved for the case of the MoS_2 monolayer, presenting a PL band that does not appear in the bulk material. The

dramatic change can be easily explained by the transformation of the indirect band gap of the bulk material to the direct electronic transition in monolayer MoS_2, which results in a highly efficient PL emission. A similar effect can be observed in the Raman spectra [89]. In relation to the electronic properties, theoretical calculations predict carrier mobility values that could guarantee monolayer TMDs applications in electronic devices [90]. Calculations for MoS_2 show electron mobilities ranging from 10–1000 $cm^2\ V^{-1}s^{-1}$ at room temperature, and even higher values surpassing $10^5\ cm^2/(Vs)$ at low temperature [91]. The experimental values were typically lower than those predicted: 0.1–10 $cm^2\ V^{-1}s^{-1}$ [92], but this discrepancy becomes considerably more pronounced for atomically thin materials because they are especially sensitive to surface condition. The most important phenomenon limiting carrier mobility is scattering with surface defects. This can be improved by two different approaches. The first one consists of the annealing of the TMD monolayers in vacuum to reduce the density of defects [93]. The second approach is analogous to the encapsulation of graphene monolayers with hBN that has already been explained above but applied to TMDs. This technique has been successfully applied to MoS_2 by using hBN [94] and also the use of HfO_2 has proven to improve MoS_2 mobility at room temperature, reaching ~150 $cm^2\ V^{-1}s^{-1}$ [95] with HfO_2 substrates or ~200 $cm^2\ V^{-1}s^{-1}$ for HfO_2 gates [92]. Apart from carrier mobility, it is also crucial to consider high-frequency capabilities when thinking about device applications. In order to obtain the best performance, the channel length (i.e., the 2D TMD layer) can be reduced to the nanometric range to take advantage of the ballistic transport. Ballistic quantum transport simulations of MoS_2 transistors have shown the possibility of achieving frequencies higher than 100 GHz using a channel length of 15 nm [96]. The first MoS_2 transistors operating at GHz frequencies showed a current-gain cut-off frequency of 6 GHz with channel lengths of 340 nm [97]. Further reduction of the channel lengths below 100 nm (gate lengths of 70 and 40 nm) together with other improvements allowed us to achieve frequencies up to 25 GHz [98].

Table 2. Outline of the experimental and theoretical bandgaps of different 2D materials. D stands for direct and I stands for indirect band gap.

2D Material		Experimental E_g (eV)			Theoretical E_g (eV)		
graphene		0			0		
h-BN		6.07	D	[74]	5.95	D	[99]
MoS_2	Bulk	1.23	I	[88]	1.23	I	[88]
	ML	1.90	D	[100]	1.76	D	[100]
$MoSe_2$	Bulk	1.09	I	[88]	1.09	I	[88]
	ML	1.57	D	[101]	1.43	D	[80]
WS_2	Bulk	1.35	I	[88]	1.32	I	[88]
	ML	1.97	D	[102]	1.95	D	[80]
WSe_2	Bulk	1.20	I	[88]	1.21	I	[88]
	ML	1.65	D	[101]	1.62	D	[80]

2.4. 2D Oxides

The 2D oxides comprise all materials formed upon the combination of O with either a metallic or quasimetallic element that presents a 2D structure. The presence of very different elements and different oxidation states result in a great richness of examples with different stoichiometry, such as ZnO, MoO_2, or MoO_3.

The most significant characteristic of 2D oxides is their stability. The presence of oxygen in their formulations results in highly stable compounds even in air. The same idea applies to the production processes that are relatively simple and have low requirements. For example, TMDs cannot be synthesized in the presence of oxygen, while many 2D oxides such as β-Ga_2O_3, β-TeO_2, and Bi_2O_3 can be manufactured by natural oxidation of the corresponding liquid metals.

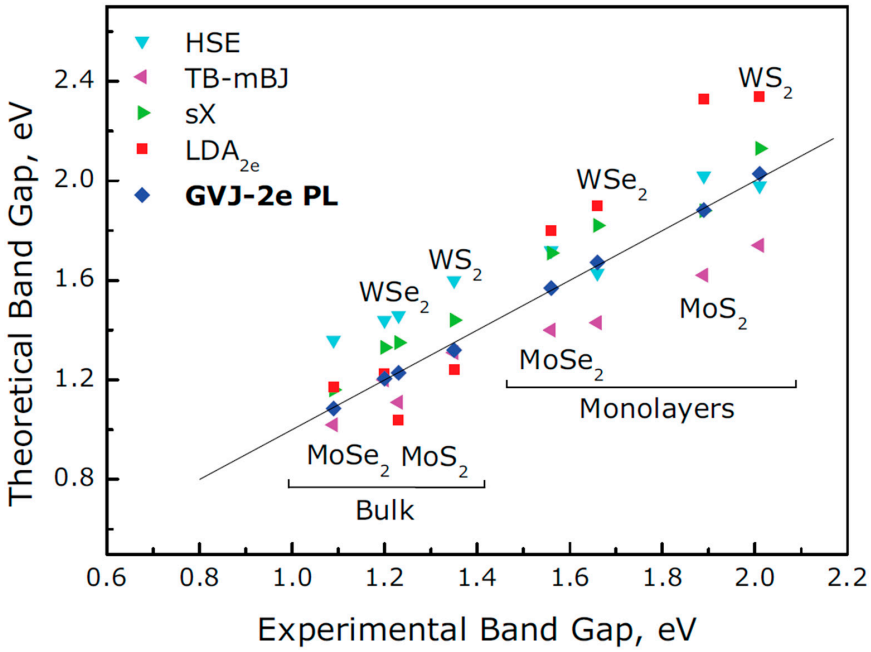

Figure 4. Theoretical and experimental band gap energies of MoS_2, WSe_2, $MoSe_2$, and WS_2. The bulk materials present lower energies, and the band gap is indirect in all cases. Reprinted (adapted) with permission from Ref. [88]. Copyright (2017) John Wiley and Sons.

The 2D oxides show recent applications in FET technology. For example, few-layer hexagonal TiO_2 has been shown to reach hole mobility of 950 $cm^2\ V^{-1}s^{-1}$ at room temperature [103]; in addition, transistors based on β-TeO_2 have shown hole mobilities over 6000 $cm^2\ V^{-1}s^{-1}$ at −50 °C together with high switching on/off ratios [104]. Nevertheless, the most productive field of 2D oxides is UV applications. 2D oxides are typically wide band gap semiconductors or even electrical insulators. As a result, most of them present direct band gap transitions in the UV region, such as ZnO. UV photodetectors based on ZnO nanosheets have shown outstanding performance, with responsivities up to 20,000 A W^{-1} for a wavelength of 254 nm [105]. Likewise, 2D β-Ga_2O_3 photodetectors show excellent wavelength selectivity with a sharp decrease of the photocurrent for wavelengths greater than 354 nm [106], exhibiting great potential for application on solar-blind photodetectors. Finally, 2D oxides have also been studied because of their use in gas sensing. For instance, a 2D MoO_3 has been used as a plasmonic H_2 sensor [107], and fully CMOS-compatible gas sensors based on SnO_2 thin films have been reported [108].

3. 1D Materials

In this section, we will take a deeper look at the optical and electric properties of 1D materials with special emphasis on the potential applications. We will focus on the distinctive properties of NWs by developing two separate subsections: one for semiconductor NWs and another one for metallic NWs.

3.1. Semiconductor NWs

As it has been previously explained, the unique properties of NWs arise from the confinement effect derived from the spatial limitation given by their diameter. When the wavelength of an incident electromagnetic (EM) field is comparable to the NW diameter, the EM confinement takes place. As a result, the optical response of the NW diverges from the behavior of the same material in bulk form. This leads to the appearance of scattering or absorption resonances for certain values of the wavelength and the NW diameter [109,110]. This has been observed in different optical phenomena such as second harmonic generation (SHG), Raman spectroscopy, or light extinction measurements. These EM resonances are

the base of all the photonic applications that will be detailed below, including lasing, solar cells, or sensors, as seen in Figure 5.

If the electrons of the material are confined, there could also be new effects in charge transport and light emission. For example, when the Bohr radius of the excitons (electron-hole pairs) is limited by the NW diameter, the photoluminescence (PL) emission can be modified [111]. In contrast, if the electron (or hole) mean free path is limited by the physical dimensions of the NW, ballistic transport can occur, resulting in the quantization of the electrical resistivity [112–114]. In the ballistic transport regime, there is no scattering, and the carriers are just reflected by the NW walls without any energy loss. Something similar occurs when the NW diameter is small enough to overcome the phonon mean free path [115]. This has an immediate effect on the thermal conductivity [116], usually causing an increase of this magnitude when confinement is present, in an analogous way to electrical conductivity in the presence of electron ballistic transport.

Another crucial property of NWs is their capability to relax mechanical stress during growth. Unlike the growth of epitaxial layers that are limited by lattice mismatch, the NW geometry is able to relieve mechanical stress and avoid the propagation of dislocations. This permits the manufacturing of heterostructures that are not possible in conventional epitaxial growth [117,118]. Heterojunctions are fundamental for the fabrication of many electronic and optoelectronic devices. Heterostructured NWs have recently been proven to add confinement of incident EM radiation in the heterojunction region and maintain the already known diameter resonances at the same time [119].

The common point of all confinement effects is the dependence of the physical properties with the confined dimension; in the case of 1D materials, this is the diameter. This relationship opens a new channel for engineering the material response and its optimization in order to face the desired applications. Another option to tailor NWs' properties is to carefully select the base material used for NW fabrication. We can use the already existing categories of semiconductors to organize the available semiconductor NWs and their applications:

3.1.1. Group IV Semiconductors

This group includes C, Si, and Ge; however, carbon (in its diamond form) is technically an insulator at room temperature because of its wide band gap of ~5.46 eV. The most relevant feature of Si and Ge NWs is their compatibility with current complementary metal oxide semiconductor (CMOS) technology. This allows us to use all the fabrication technology developed around bulk Si to these NWs and facilitates the integration of novel NW-based devices with already existing technologies.

The main attributes of group IV semiconductor NWs are their low band gap, their natural availability on the Earth's surface, and their well-known manufacturing process. All of these factors make them suitable for the fabrication of transistors for basic electronics [1,120,121] and photovoltaic devices [122–124]. The main drawbacks are low carrier mobility, which limits its use on high-frequency electronics, and the indirect band gap, which hinders their light-emitting capabilities and the possible applications on lasers or light emitting diodes (LEDs).

3.1.2. Group III–V Semiconductors

The III–V semiconductors include all combinations of elements of the groups III and V, such as GaAs, InAs, InP, GaN, etc. The strong points of this group complement those of group IV. They present a direct band gap in the visible and near-infrared regions, which makes them suitable for the manufacturing of LEDs, lasers, solar cells, or other NW-based optoelectronic devices [125]. Particularly, in the photovoltaics field, InP NWs solar cells have been shown to achieve a 13.8% efficiency [126]; more recently, a GaAs NW solar cell reached 15.3% efficiency [127]. They also present much higher carrier mobilities than group IV semiconductors opening interesting applications for high-frequency electronics [128]. Finally, the possibility of growing ternary or even quaternary combinations of these com-

pounds, such as $In_xGa_{(1-x)}As$, $Al_xGa_{(1-x)}As$, or $Al_xGa_yIn_{(1-x-y)}P$, permits the continuous tunability of properties such as the band gap or the refractive index [129].

3.1.3. Semiconductor Metal Oxides

We can find several metal oxides that behave as semiconductors in nature, such as ZnO, SnO_2, CuO, TiO_2, or Ga_2O_3, among others [130]. ZnO NWs attracted a lot of attention because of their easy manufacturing process and their efficient 3.3 eV emission just on the onset of the UV region, which makes them suitable for the fabrication of UV and blue LEDs [131]. Another application of many metal oxide semiconductor NWs is on gas sensors by taking advantage of the EM field localization near the NW or the sensitivity of the NW resistivity to modifications of its surface [132]. In addition, the high surface–volume ratio of the NW geometry helps to improve the response of this kind of device, which can be further optimized through surface functionalization.

3.1.4. Group II–VI Semiconductors

The last group we will consider is group II–VI semiconductor NWs. It is comprised of semiconductors such as ZnS, ZnSe, ZnTe, CdS, or CdSe, and also technically ZnO, even though it has been considered in the group of metal oxides. They are well known because of their light-emitting properties arising from their direct band gap transition in the visible range: 1.70 eV for CdSe or 2.42 eV for CdS [133]. Even if its application in bulk form and thin films has been limited because of the low defect requirements for epitaxial growth, this is no longer a problem for NWs that present excellent crystalline quality and easier and controlled doping [129,133,134].

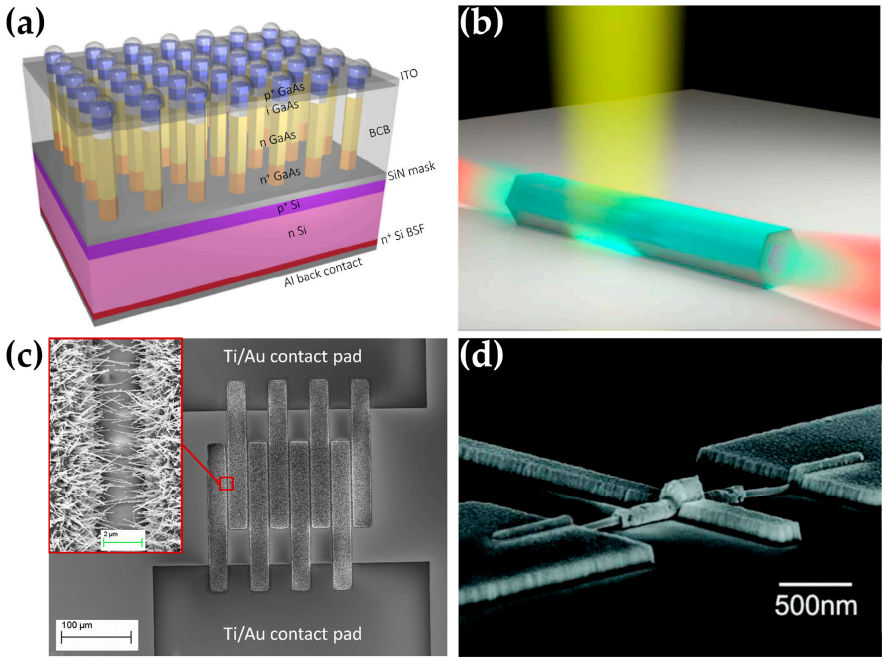

Figure 5. Different technological applications of semiconductor NWs. (**a**) Schematic of a GaAs NW-based solar cell. Reprinted (adapted) with permission from Ref. [135]. Copyright (2015) American Chemical Society. (**b**) GaAs/InGaAs NW laser concept. Reproduced from the publication of Yi et al. [136] with no modification under Creative Commons 4.0 license (https://creativecommons.org/licenses/by/4.0/, accessed on 1 December 2022). (**c**) CuO NWs gas sensor. Reprinted from Ref. [137], Copyright (2013), with permission from Elsevier. (**d**) SEM image of an InAs FET. Reprinted (adapted) with permission from Ref. [138]. Copyright (2012) American Chemical Society.

3.2. Metallic NWs

Metallic NWs excel for their excellent thermal and electrical conductivity, the ability to show optical transparency, and their flexibility [139]. The immediate application of all these properties is for transparent conductive electrodes (TCEs), as seen in Figure 6. Their excellent electrical conductivity coming from their metallic nature, together with the optical transparency, permits the manufacturing of films formed by dense networks of Ag, Au, or Cu NWs [140–143]. This new technology could be used to substitute the current TCE leader, indium tin oxide (ITO), which is more expensive and naturally brittle, which prevents its application in flexible device technologies. Along this line, the use of metallic NWs has contributed to the development of new wearable electronic devices [144].

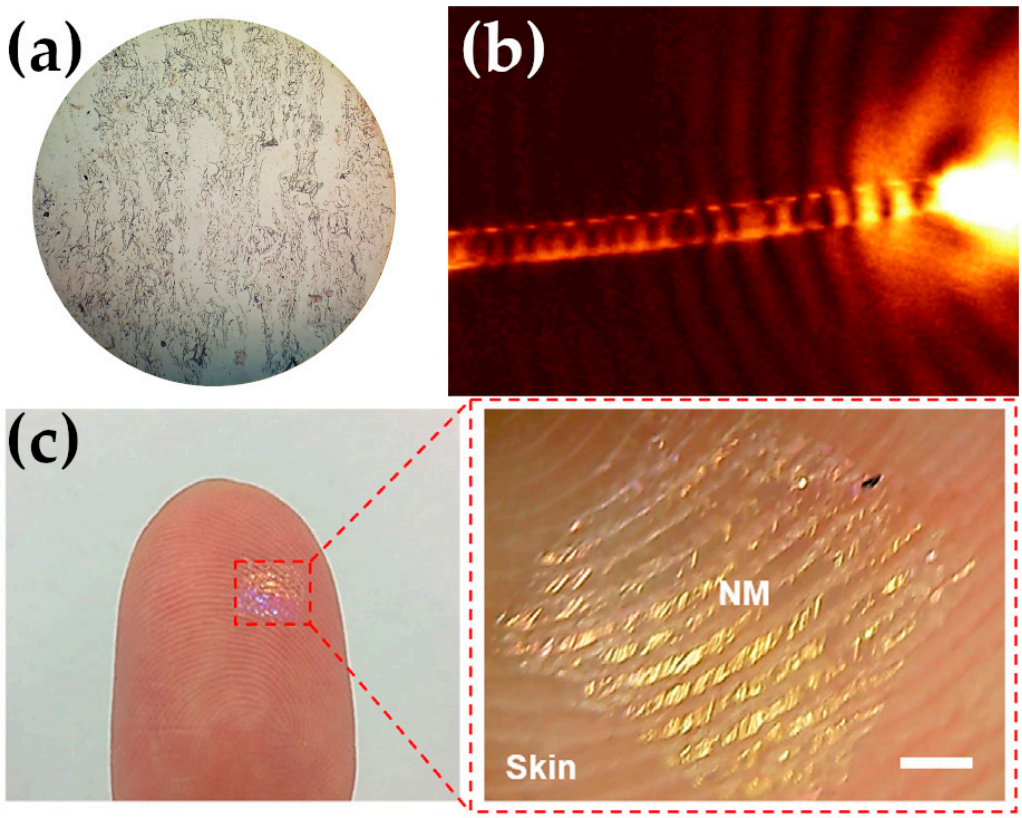

Figure 6. (**a**) Optical image of an ITO substrate covered with a Ag NWs transparent film. (**b**) Scanning near-field optical microscopy (SNOM) image of the propagation of a surface plasmon along an 18:6 μm long Ag NW. Reprinted figure with permission from Ref. [145]. Copyright (2005) by the American Physical Society. http://dx.doi.org/10.1103/PhysRevLett.95.257403 (accessed on 1 December 2022). (**c**) Hybrid PDMS/AgNWs conductive nanomembrane attached to a thumb. Scale bar is 1 mm. Reproduced from Ref. [146] with no modification under Creative Commons 4.0 license (https://creativecommons.org/licenses/by/4.0/, accessed on 1 December 2022).

The exceptional electrical conductivity can be used together with their inherently high surface/volume ratio arising from its 1D nature to boost the performance of electrochemical sensors [147,148]. On one hand, the high surface/volume ratio improves the sensitive area of the sensor, thus enhancing the signal intensity. On the other hand, the electric conductivity of the metallic NW improves the charge movement of the electrodes, and under certain circumstances, they can improve the charge transfer process during the redox reactions enabling direct electron transfer (DET) [149]. Another interesting capability of NW-based sensors is the possibility of functionalization of the NWs' surface with different organic molecules such as enzymes. This kind of modification enhances the sensitivity of the sensor and unlocks a new way to design biosensors that react in a specific way to certain molecules [149,150].

Another fascinating property of metallic NWs is the plasmonic resonances that result in the localization of the electromagnetic field on its surface. This allows us to enhance any possible optical effects that take place in this region. If we combine this effect with Raman spectroscopy, we could be able to place certain molecules over the NW surface and we will observe a dramatic increase in its Raman signal. This technique is named surface-enhanced Raman spectroscopy (SERS) and appears when working with metallic NWs, as well as for metallic nanoparticles [151,152]. SERS permits to detect very small amounts of materials and, for example, has been employed recently to improve MoS_2 Raman signal [153].

In a similar fashion, plasmonic resonances can be utilized for light control in photonic devices. Ag NWs can be applied to fabricate plasmonic waveguides [145,154], as seen in Figure 6b. In these structures, the EM field travels mostly over the NW surface in an evanescent wave, which allows the coupling of the NW waveguide to other optical fibers or other NWs waveguides to form optical circuits and devices. Ag NWs have also been used to fabricate plasmonic metasurfaces [155] or even plasmonic gratings that produce structural color [156].

4. Concluding Remarks

In this review, we presented a general overview of the novel physical properties of low-dimensional materials together with the innovative applications derived from them. The different types of low-dimensional materials have been organized in accordance with their respective dimensionality, with the review being focused mainly on 2D and 1D materials. In both cases, the emergence of their respective groundbreaking properties has been rationalized as a consequence of the confinement of the corresponding physical dimensions.

The innovative applications of low-dimensional materials in the fields of electronics and photonics have been highlighted. Atomically thin 2D materials excel in transistor technologies, either as the transistor channel, such as graphene, or as dielectrics, such as hBN. Alternatively, TMDs present high carrier mobilities, which is interesting for FET applications, as well as direct band gaps in the visible range, allowing their use as light emitters. The 2D oxides have been shown to stand out in UV applications, especially as photodetectors. In contrast, semiconductor NWs based on group IV materials have been shown to be suitable for photovoltaic applications and electronics, being compatible with current CMOS technologies. Semiconductor NWs from groups III–V or II–VI present other capabilities such as better carrier mobilities that are interesting for fast electronics, and efficient light emissions for photonic devices. Finally, metallic NWs excel because of their excellent electrical conductivity and their optical transparency, which defines their interest in TCEs and electrochemical sensors. In addition, the presence of strong plasmonic resonances opens their applicability to technologies such as SERS, waveguiding, or metasurfaces.

Funding: This research was funded by the European Union–NextGenerationEU and the University of Valladolid, within the Margarita Salas program, grant number CONVREC-2021-23.

Data Availability Statement: Not applicable.

Acknowledgments: The author would like to acknowledge Irene Mediavilla for her comments on the manuscript and fruitful discussion.

Conflicts of Interest: The author declares no conflict of interest.

References

1. Lu, W.; Xie, P.; Lieber, C.M. Nanowire transistor performance limits and applications. *IEEE Trans. Electron Devices* **2008**, *55*, 2859–2876. [CrossRef]
2. Schwierz, F.; Pezoldt, J.; Granzner, R. Two-dimensional materials and their prospects in transistor electronics. *Nanoscale* **2015**, *7*, 8261–8283. [CrossRef] [PubMed]
3. Das, S.; Sebastian, A.; Pop, E.; McClellan, C.J.; Franklin, A.D.; Grasser, T.; Knobloch, T.; Illarionov, Y.; Penumatcha, A.V.; Appenzeller, J.; et al. Transistors based on two-dimensional materials for future integrated circuits. *Nat. Electron.* **2021**, *4*, 786–799. [CrossRef]

4. Tian, B.; Zheng, X.; Kempa, T.J.; Fang, Y.; Yu, N.; Yu, G.; Huang, J.; Lieber, C.M. Coaxial silicon nanowires as solar cells and nanoelectronic power sources. *Nature* **2007**, *449*, 885–889. [CrossRef] [PubMed]
5. Tanabe, K. A review of ultrahigh efficiency III-V semiconductor compound solar cells: Multijunction tandem, lower dimensional, photonic up/down conversion and plasmonic nanometallic structures. *Energies* **2009**, *2*, 504–530. [CrossRef]
6. Chao, L.; Wang, Z.; Xia, Y.; Chen, Y.; Huang, W. Recent progress on low dimensional perovskite solar cells. *J. Energy Chem.* **2018**, *27*, 1091–1100. [CrossRef]
7. Chan, C.K.; Peng, H.; Liu, G.; McIlwrath, K.; Zhang, X.F.; Huggins, R.A.; Cui, Y. High-performance lithium battery anodes using silicon nanowires. *Nat. Nanotechnol.* **2007**, *3*, 31–35. [CrossRef]
8. Bo, T.; Liu, P.F.; Zhang, J.; Wang, F.; Wang, B.T. Tetragonal and trigonal Mo2B2 monolayers: Two new low-dimensional materials for Li-ion and Na-ion batteries. *Phys. Chem. Chem. Phys.* **2019**, *21*, 5178–5188. [CrossRef]
9. Peng, L.; Zhu, Y.; Chen, D.; Ruoff, R.S.; Yu, G. Two-Dimensional Materials for Beyond-Lithium-Ion Batteries. *Adv. Energy Mater.* **2016**, *6*, 1600025. [CrossRef]
10. Greytak, A.B.; Barrelet, C.J.; Li, Y.; Lieber, C.M. Semiconductor nanowire laser and nanowire waveguide electro-optic modulators. *Appl. Phys. Lett.* **2005**, *87*, 151103. [CrossRef]
11. Odoh, E.O.; Njapba, A.S. A Review of Semiconductor Quantum Well Devices. *Adv. Phys. Theor. Appl.* **2015**, *46*, 26–32.
12. Yin, Y.; Qiu, T.; Li, J.; Chu, P.K. Plasmonic nano-lasers. *Nano Energy* **2012**, *1*, 25–41. [CrossRef]
13. Qu, X.; Alvarez, P.J.J.; Li, Q. Applications of nanotechnology in water and wastewater treatment. *Water Res.* **2013**, *47*, 3931–3946. [CrossRef] [PubMed]
14. Kolmakov, A.; Zhang, Y.; Cheng, G.; Moskovits, M. Detection of CO and O_2 using tin oxide nanowire sensors. *Adv. Mater.* **2003**, *15*, 997–1000. [CrossRef]
15. Bogue, R. Graphene sensors: A review of recent developments. *Sens. Rev.* **2014**, *34*, 233–238. [CrossRef]
16. Farokhzad, O.C.; Langer, R. Impact of nanotechnology on drug delivery. *ACS Nano* **2009**, *3*, 16–20. [CrossRef]
17. Ferrari, M. Cancer nanotechnology: Opportunities and challenges. *Nat. Rev. Cancer* **2005**, *5*, 161–171. [CrossRef]
18. Klitzing, K.V.; Dorda, G.; Pepper, M. New method for high-accuracy determination of the fine-structure constant based on quantized hall resistance. *Phys. Rev. Lett.* **1980**, *45*, 494–497. [CrossRef]
19. Holonyak, N.; Kolbas, R.M.; Dupuis, R.D.; Dapkus, P.D. Quantum-Well Heterostructure Lasers. *IEEE J. Quantum Electron.* **1980**, *16*, 170–186. [CrossRef]
20. Levine, B.F. Quantum-well infrared photodetectors. *J. Appl. Phys.* **1993**, *74*, R1–R81. [CrossRef]
21. Tang, Q.; Zhou, Z. Graphene-analogous low-dimensional materials. *Prog. Mater. Sci.* **2013**, *58*, 1244–1315. [CrossRef]
22. Lu, W.; Lieber, C.M. Semiconductor nanowires. *J. Phys. D. Appl. Phys.* **2006**, *39*, R387–R406. [CrossRef]
23. Agarwal, R.; Lieber, C.M. Semiconductor nanowires: Optics and optoelectronics. *Appl. Phys. A Mater. Sci. Process.* **2006**, *85*, 209–215. [CrossRef]
24. Lal, S.; Hafner, J.H.; Halas, N.J. Noble Metal Nanowires: From Plasmon. *Acc. Chem. Res.* **2012**, *45*, 1887–1895. [CrossRef] [PubMed]
25. Kim, M.J.; Cruz, M.A.; Yang, F.; Wiley, B.J. Accelerating electrochemistry with metal nanowires. *Curr. Opin. Electrochem.* **2019**, *16*, 19–27. [CrossRef]
26. Holzman, I.; Ivry, Y. Superconducting Nanowires for Single-Photon Detection: Progress, Challenges, and Opportunities. *Adv. Quantum Technol.* **2019**, *2*, 1800058. [CrossRef]
27. Krogstrup, P.; Ziino, N.L.B.; Chang, W.; Albrecht, S.M.; Madsen, M.H.; Johnson, E.; Nygård, J.; Marcus, C.M.; Jespersen, T.S. Epitaxy of semiconductor-superconductor nanowires. *Nat. Mater.* **2015**, *14*, 400–406. [CrossRef]
28. Jayaraman, K.; Kotaki, M.; Zhang, Y.; Mo, X.; Ramakrishna, S. Recent Advances in Polymer Nanofibers. *J. Nanosci. Nanotechnol.* **2004**, *4*, 52–65. [CrossRef]
29. Thostenson, E.T.; Ren, Z.; Chou, T.-W. Advances in the science and technology of carbon nanotubes and their composites: A review. *Compos. Sci. Technol.* **2001**, *61*, 1899–1912. [CrossRef]
30. Tang, Y.H.; Pei, L.Z.; Chen, Y.W.; Guo, C. Self-assembled silicon nanotubes under supercritically hydrothermal conditions. *Phys. Rev. Lett.* **2005**, *95*, 116102. [CrossRef]
31. Zhao, J.; Wei, W.; Xu, N.; Wang, X.; Chang, L.; Wang, L.; Fang, L.; Le, Z.; Nie, P. Dealloying Synthesis of Silicon Nanotubes for High-Performance Lithium Ion Batteries. *ChemPhysChem* **2022**, *23*, e202100832. [CrossRef] [PubMed]
32. Zhi, C.; Bando, Y.; Tang, C.; Golberg, D. Boron nitride nanotubes. *Mater. Sci. Eng. R Rep.* **2010**, *70*, 92–111. [CrossRef]
33. Zhi, C.Y.; Bai, X.D.; Wang, E.G. Boron carbonitride nanotubes. *J. Nanosci. Nanotechnol.* **2004**, *4*, 35–51. [CrossRef] [PubMed]
34. Yesilbag, Y.O.; Tuzluca Yesilbag, F.N.; Huseyin, A.; Ertugrul, M. The hierarchical synthesis of tungsten disulfide coated vertically aligned boron carbon nitride nanotubes composite electrodes for supercapacitors. *J. Energy Storage* **2022**, *52*, 104964. [CrossRef]
35. Ealias, A.M.; Saravanakumar, M.P. A review on the classification, characterisation, synthesis of nanoparticles and their application. *IOP Conf. Ser. Mater. Sci. Eng.* **2017**, *263*, 032019. [CrossRef]
36. Mitchell, M.J.; Billingsley, M.M.; Haley, R.M.; Wechsler, M.E.; Peppas, N.A.; Langer, R. Engineering precision nanoparticles for drug delivery. *Nat. Rev. Drug Discov.* **2021**, *20*, 101–124. [CrossRef]
37. Dingle, R.; Wiegmann, W.; Henry, C.H. Quantum states of confined carriers in very thin AlxGa1-xAs-GaAs-AlxGa1-xAs heterostructures. *Phys. Rev. Lett.* **1974**, *33*, 827–830. [CrossRef]
38. White, C.T.; Mintmire, J.W. Density of states reflects diameter in nanotubes. *Nature* **1998**, *394*, 29–30. [CrossRef]

39. Hook, J.R. *Solid State Physics*, 2nd ed.; Hall, H.E., Ed.; John Wiley and Sons: Chichester, UK, 2004; ISBN 0-471-92805-4.
40. Kittel, C. *Introduction to Solid State Physics*, 8th ed.; Wiley: Hoboken, NJ, USA, 2004; ISBN 978-0-471-41526-8.
41. Geim, A.K.; Grigorieva, I.V. Van der Waals heterostructures. *Nature* **2013**, *499*, 419–425. [CrossRef]
42. Hu, X.; Liu, K.; Cai, Y.; Zang, S.-Q.; Zhai, T. 2D Oxides for Electronics and Optoelectronics. *Small Sci.* **2022**, *2*, 2200008. [CrossRef]
43. Geim, A.K.; Novoselov, K.S. The rise of graphene. In *Nanoscience and Technology*; Co-Published with Macmillan Publishers Ltd.: New York, NY, USA, 2009; Volume 6, pp. 11–19. [CrossRef]
44. Castro Neto, A.H.; Guinea, F.; Peres, N.M.R.; Novoselov, K.S.; Geim, A.K. The electronic properties of graphene. *Rev. Mod. Phys.* **2009**, *81*, 109–162. [CrossRef]
45. Novoselov, K.S.; Geim, A.K.; Morozov, S.V.; Jiang, D.; Zhang, Y.; Dubonos, S.V.; Grigorieva, I.V.; Firsov, A.A. Electric Field Effect in Atomically Thin Carbon Films. *Science* **2004**, *306*, 666–669. [CrossRef] [PubMed]
46. Kuzmenko, A.B.; Van Heumen, E.; Carbone, F.; Van Der Marel, D. Universal optical conductance of graphite. *Phys. Rev. Lett.* **2008**, *100*, 2–5. [CrossRef]
47. Nair, R.R.; Ren, W.; Jalil, R.; Riaz, I.; Kravets, V.G.; Britnell, L.; Blake, P.; Schedin, F.; Mayorov, A.S.; Yuan, S.; et al. Fluorographene: A two-dimensional counterpart of Teflon. *Small* **2010**, *6*, 2877–2884. [CrossRef] [PubMed]
48. Cao, Y.; Fatemi, V.; Demir, A.; Fang, S.; Tomarken, S.L.; Luo, J.Y.; Sanchez-Yamagishi, J.D.; Watanabe, K.; Taniguchi, T.; Kaxiras, E.; et al. Correlated insulator behaviour at half-filling in magic-angle graphene superlattices. *Nature* **2018**, *556*, 80–84. [CrossRef] [PubMed]
49. Cao, Y.; Fatemi, V.; Fang, S.; Watanabe, K.; Taniguchi, T.; Kaxiras, E.; Jarillo-Herrero, P. Unconventional superconductivity in magic-angle graphene superlattices. *Nature* **2018**, *556*, 43–50. [CrossRef]
50. Geim, A.K. Graphene: Status and Prospects. *Science* **2009**, *324*, 1530–1534. [CrossRef] [PubMed]
51. Choi, W.; Lahiri, I.; Seelaboyina, R.; Kang, Y.S. Synthesis of graphene and its applications: A review. *Crit. Rev. Solid State Mater. Sci.* **2010**, *35*, 52–71. [CrossRef]
52. Novoselov, K.S.; Fal'Ko, V.I.; Colombo, L.; Gellert, P.R.; Schwab, M.G.; Kim, K. A roadmap for graphene. *Nature* **2012**, *490*, 192–200. [CrossRef]
53. Pumera, M.; Sofer, Z. Towards stoichiometric analogues of graphene: Graphane, fluorographene, graphol, graphene acid and others. *Chem. Soc. Rev.* **2017**, *46*, 4450–4463. [CrossRef]
54. Chronopoulos, D.D.; Bakandritsos, A.; Pykal, M.; Zbořil, R.; Otyepka, M. Chemistry, properties, and applications of fluorographene. *Appl. Mater. Today* **2017**, *9*, 60–70. [CrossRef] [PubMed]
55. Park, S.; Ruoff, R.S. Chemical methods for the production of graphenes. *Nat. Nanotechnol.* **2009**, *4*, 217–224. [CrossRef]
56. Eda, G.; Chhowalla, M. Chemically derived graphene oxide: Towards large-area thin-film electronics and optoelectronics. *Adv. Mater.* **2010**, *22*, 2392–2415. [CrossRef] [PubMed]
57. Dikin, D.A.; Stankovich, S.; Zimney, E.J.; Piner, R.D.; Dommett, G.H.B.; Evmenenko, G.; Nguyen, S.T.; Ruoff, R.S. Preparation and characterization of graphene oxide paper. *Nature* **2007**, *448*, 457–460. [CrossRef] [PubMed]
58. Robinson, J.T.; Zalalutdinov, M.; Baldwin, J.W.; Snow, E.S.; Wei, Z.; Sheehan, P.; Houston, B.H. Wafer-scale reduced graphene oxide films for nanomechanical devices. *Nano Lett.* **2008**, *8*, 3441–3445. [CrossRef]
59. Becerril, H.A.; Mao, J.; Liu, Z.; Stoltenberg, R.M.; Bao, Z.; Chen, Y. Evaluation of solution-processed reduced graphene oxide films as transparent conductors. *ACS Nano* **2008**, *2*, 463–470. [CrossRef]
60. Jin, M.; Jeong, H.K.; Yu, W.J.; Bae, D.J.; Kang, B.R.; Lee, Y.H. Graphene oxide thin film field effect transistors without reduction. *J. Phys. D Appl. Phys.* **2009**, *42*, 135109. [CrossRef]
61. Mattevi, C.; Eda, G.; Agnoli, S.; Miller, S.; Mkhoyan, K.A.; Celik, O.; Mastrogiovanni, D.; Granozzi, G.; Carfunkel, E.; Chhowalla, M. Evolution of electrical, chemical, and structural properties of transparent and conducting chemically derived graphene thin films. *Adv. Funct. Mater.* **2009**, *19*, 2577–2583. [CrossRef]
62. Eda, G.; Fanchini, G.; Chhowalla, M. Large-area ultrathin films of reduced graphene oxide as a transparent and flexible electronic material. *Nat. Nanotechnol.* **2008**, *3*, 270–274. [CrossRef]
63. Stankovich, S.; Dikin, D.A.; Piner, R.D.; Kohlhaas, K.A.; Kleinhammes, A.; Jia, Y.; Wu, Y.; Nguyen, S.B.T.; Ruoff, R.S. Synthesis of graphene-based nanosheets via chemical reduction of exfoliated graphite oxide. *Carbon* **2007**, *45*, 1558–1565. [CrossRef]
64. López, V.; Sundaram, R.S.; Gómez-Navarro, C.; Olea, D.; Burghard, M.; Gómez-Herrero, J.; Zamora, F.; Kern, K. Chemical vapor deposition repair of graphene oxide: A route to highly conductive graphene monolayers. *Adv. Mater.* **2009**, *21*, 4683–4686. [CrossRef]
65. Liu, Q.; Liu, Z.; Zhang, X.; Yang, L.; Zhang, N.; Pan, G.; Yin, S.; Chen, Y.; Wei, J. Polymer photovoltaic cells based on solution-processable graphene and P3HT. *Adv. Funct. Mater.* **2009**, *19*, 894–904. [CrossRef]
66. Lv, X.; Huang, Y.; Liu, Z.; Tian, J.; Wang, Y.; Ma, Y.; Liang, J.; Fu, S.; Wan, X.; Chen, Y. Photoconductivity of bulk-film-based graphene sheets. *Small* **2009**, *5*, 1682–1687. [CrossRef] [PubMed]
67. Eda, G.; Chhowalla, M. Graphene-based composite thin films for electronics. *Nano Lett.* **2009**, *9*, 814–818. [CrossRef]
68. Eda, G.; Lin, Y.Y.; Miller, S.; Chen, C.W.; Su, W.F.; Chhowalla, M. Transparent and conducting electrodes for organic electronics from reduced graphene oxide. *Appl. Phys. Lett.* **2008**, *92*, 10–13. [CrossRef]
69. Zhu, Y.; Cai, W.; Piner, R.D.; Velamakanni, A.; Ruoff, R.S. Transparent self-assembled films of reduced graphene oxide platelets. *Appl. Phys. Lett.* **2009**, *95*, 103104. [CrossRef]

70. Pang, S.; Tsao, H.N.; Feng, X.; Mullen, K. Patterned graphene electrodes from solution-processed graphite oxide films for organic field-effect transistors. *Adv. Mater.* **2009**, *21*, 3488–3491. [CrossRef]
71. Arsat, R.; Breedon, M.; Shafiei, M.; Spizziri, P.G.; Gilje, S.; Kaner, R.B.; Kalantar-zadeh, K.; Wlodarski, W. Graphene-like nano-sheets for surface acoustic wave gas sensor applications. *Chem. Phys. Lett.* **2009**, *467*, 344–347. [CrossRef]
72. Fowler, J.D.; Allen, M.J.; Tung, V.C.; Yang, Y.; Kaner, R.B.; Weiller, B.H. Practical chemical sensors from chemically derived graphene. *ACS Nano* **2009**, *3*, 301–306. [CrossRef]
73. Zhou, M.; Zhai, Y.; Dong, S. Electrochemical sensing and biosensing platform based on chemically reduced graphene oxide. *Anal. Chem.* **2009**, *81*, 5603–5613. [CrossRef]
74. Kim, K.K.; Hsu, A.; Jia, X.; Kim, S.M.; Shi, Y.; Hofmann, M.; Nezich, D.; Rodriguez-Nieva, J.F.; Dresselhaus, M.; Palacios, T.; et al. Synthesis of monolayer hexagonal boron nitride on Cu foil using chemical vapor deposition. *Nano Lett.* **2012**, *12*, 161–166. [CrossRef] [PubMed]
75. Zhang, K.; Feng, Y.; Wang, F.; Yang, Z.; Wang, J. Two dimensional hexagonal boron nitride (2D-hBN): Synthesis, properties and applications. *J. Mater. Chem. C* **2017**, *5*, 11992–12022. [CrossRef]
76. Dean, C.R.; Young, A.F.; Meric, I.; Lee, C.; Wang, L.; Sorgenfrei, S.; Watanabe, K.; Taniguchi, T.; Kim, P.; Shepard, K.L.; et al. Boron nitride substrates for high-quality graphene electronics. *Nat. Nanotechnol.* **2010**, *5*, 722–726. [CrossRef]
77. Wang, H.; Taychatanapat, T.; Hsu, A.; Watanabe, K.; Taniguchi, T.; Jarillo-Herrero, P.; Palacios, T. BN/Graphene/BN transistors for RF applications. *IEEE Electron Device Lett.* **2011**, *32*, 1209–1211. [CrossRef]
78. Lee, G.H.; Yu, Y.J.; Cui, X.; Petrone, N.; Lee, C.H.; Choi, M.S.; Lee, D.Y.; Lee, C.; Yoo, W.J.; Watanabe, K.; et al. Flexible and transparent MoS2 field-effect transistors on hexagonal boron nitride-graphene heterostructures. *ACS Nano* **2013**, *7*, 7931–7936. [CrossRef]
79. Chang, C.H.; Fan, X.; Lin, S.H.; Kuo, J.L. Orbital analysis of electronic structure and phonon dispersion in MoS 2, MoSe2, WS2, and WSe2 monolayers under strain. *Phys. Rev. B-Condens. Matter Mater. Phys.* **2013**, *88*, 195420. [CrossRef]
80. Deng, S.; Li, L.; Li, M. Stability of direct band gap under mechanical strains for monolayer MoS2, MoSe2, WS2 and WSe2. *Phys. E Low-Dimens. Syst. Nanostruct.* **2018**, *101*, 44–49. [CrossRef]
81. Wilson, J.A.; Yoffe, A.D. The transition metal dichalcogenides discussion and interpretation of the observed optical, electrical and structural properties. *Adv. Phys.* **1969**, *18*, 193–335. [CrossRef]
82. Gusakova, J.; Wang, X.; Shiau, L.L.; Krivosheeva, A.; Shaposhnikov, V.; Borisenko, V.; Gusakov, V.; Tay, B.K. Electronic Properties of Bulk and Monolayer TMDs: Theoretical Study Within DFT Framework (GVJ-2e Method). *Phys. Status Solidi Appl. Mater. Sci.* **2017**, *214*, 1700218. [CrossRef]
83. Xi, X.; Wang, Z.; Zhao, W.; Park, J.H.; Law, K.T.; Berger, H.; Forró, L.; Shan, J.; Mak, K.F. Ising pairing in superconducting NbSe2 atomic layers. *Nat. Phys.* **2016**, *12*, 139–143. [CrossRef]
84. Lu, J.M.; Zheliuk, O.; Leermakers, I.; Yuan, N.F.Q.; Zeitler, U.; Law, K.T.; Ye, J.T. Evidence for two-dimensional Ising superconductivity in gated MoS2. *Science* **2015**, *350*, 1353–1357. [CrossRef]
85. Liu, C.X. Unconventional Superconductivity in Bilayer Transition Metal Dichalcogenides. *Phys. Rev. Lett.* **2017**, *118*, 087001. [CrossRef] [PubMed]
86. Sajadi, E.; Palomaki, T.; Fei, Z.; Zhao, W.; Bement, P.; Olsen, C.; Luescher, S.; Xu, X.; Folk, J.A.; Cobden, D.H. Gate-induced superconductivity in a monolayer topological insulator. *Science* **2018**, *362*, 922–925. [CrossRef]
87. Fei, Z.; Palomaki, T.; Wu, S.; Zhao, W.; Cai, X.; Sun, B.; Nguyen, P.; Finney, J.; Xu, X.; Cobden, D.H. Edge conduction in monolayer WTe 2. *Nat. Phys.* **2017**, *13*, 677–682. [CrossRef]
88. Sun, B.; Zhao, W.; Palomaki, T.; Fei, Z.; Runburg, E.; Malinowski, P.; Huang, X.; Cenker, J.; Cui, Y.T.; Chu, J.H.; et al. Evidence for equilibrium exciton condensation in monolayer WTe2. *Nat. Phys.* **2022**, *18*, 94–99. [CrossRef]
89. Splendiani, A.; Sun, L.; Zhang, Y.; Li, T.; Kim, J.; Chim, C.Y.; Galli, G.; Wang, F. Emerging photoluminescence in monolayer MoS2. *Nano Lett.* **2010**, *10*, 1271–1275. [CrossRef] [PubMed]
90. Manzeli, S.; Ovchinnikov, D.; Pasquier, D.; Yazyev, O.V.; Kis, A. 2D transition metal dichalcogenides. *Nat. Rev. Mater.* **2017**, *2*, 17033. [CrossRef]
91. Kaasbjerg, K.; Thygesen, K.S.; Jacobsen, K.W. Phonon-limited mobility in n-type single-layer MoS 2 from first principles. *Phys. Rev. B-Condens. Matter Mater. Phys.* **2012**, *85*, 115317. [CrossRef]
92. Radisavljevic, B.; Radenovic, A.; Brivio, J.; Giacometti, V.; Kis, A. Single-layer MoS2 transistors. *Nat. Nanotechnol.* **2011**, *6*, 147–150. [CrossRef]
93. Radisavljevic, B.; Kis, A. Mobility engineering and a metal-insulator transition in monolayer MoS 2. *Nat. Mater.* **2013**, *12*, 815–820. [CrossRef]
94. Cui, X.; Lee, G.H.; Kim, Y.D.; Arefe, G.; Huang, P.Y.; Lee, C.H.; Chenet, D.A.; Zhang, X.; Wang, L.; Ye, F.; et al. Multi-terminal transport measurements of MoS2 using a van der Waals heterostructure device platform. *Nat. Nanotechnol.* **2015**, *10*, 534–540. [CrossRef] [PubMed]
95. Yu, Z.; Ong, Z.Y.; Pan, Y.; Cui, Y.; Xin, R.; Shi, Y.; Wang, B.; Wu, Y.; Chen, T.; Zhang, Y.W.; et al. Realization of Room-Temperature Phonon-Limited Carrier Transport in Monolayer MoS2 by Dielectric and Carrier Screening. *Adv. Mater.* **2016**, *28*, 547–552. [CrossRef] [PubMed]
96. Yoon, Y.; Ganapathi, K.; Salahuddin, S. How good can monolayer MoS2 transistors be? *Nano Lett.* **2011**, *11*, 3768–3773. [CrossRef]

97. Krasnozhon, D.; Lembke, D.; Nyffeler, C.; Leblebici, Y.; Kis, A. MoS2 transistors operating at gigahertz frequencies. *Nano Lett.* **2014**, *14*, 5905–5911. [CrossRef] [PubMed]
98. Krasnozhon, D.; Dutta, S.; Nyffeler, C.; Leblebici, Y.; Kis, A. High-frequency, scaled MoS2 transistors. In Proceedings of the 2015 IEEE International Electron Devices Meeting (IEDM), Washington, DC, USA, 7–9 December 2015; IEEE: Piscataway, NJ, USA, 2015; pp. 27.4.1–27.4.4. [CrossRef]
99. Blase, X.; Rubio, A.; Louie, S.G.; Cohen, M.L. Quasiparticle band structure of bulk hexagonal boron nitride and related systems. *Phys. Rev. B* **1995**, *51*, 6868–6875. [CrossRef] [PubMed]
100. Mak, K.F.; Lee, C.; Hone, J.; Shan, J.; Heinz, T.F. Atomically thin MoS2: A new direct-gap semiconductor. *Phys. Rev. Lett.* **2010**, *105*, 2–5. [CrossRef] [PubMed]
101. Tonndorf, P.; Schmidt, R.; Böttger, P.; Zhang, X.; Börner, J.; Liebig, A.; Albrecht, M.; Kloc, C.; Gordan, O.; Zahn, D.R.T.; et al. Photoluminescence emission and Raman response of monolayer MoS_2, MoSe_2, and WSe_2. *Opt. Express* **2013**, *21*, 4908. [CrossRef]
102. Gutiérrez, H.R.; Perea-López, N.; Elías, A.L.; Berkdemir, A.; Wang, B.; Lv, R.; López-Urías, F.; Crespi, V.H.; Terrones, H.; Terrones, M. Extraordinary room-temperature photoluminescence in triangular WS 2 monolayers. *Nano Lett.* **2013**, *13*, 3447–3454. [CrossRef]
103. Zhang, B.Y.; Xu, K.; Yao, Q.; Jannat, A.; Ren, G.; Field, M.R.; Wen, X.; Zhou, C.; Zavabeti, A.; Ou, J.Z. Hexagonal metal oxide monolayers derived from the metal–gas interface. *Nat. Mater.* **2021**, *20*, 1073–1078. [CrossRef]
104. Zavabeti, A.; Aukarasereenont, P.; Tuohey, H.; Syed, N.; Jannat, A.; Elbourne, A.; Messalea, K.A.; Zhang, B.Y.; Murdoch, B.J.; Partridge, J.G.; et al. High-mobility p-type semiconducting two-dimensional β-TeO2. *Nat. Electron.* **2021**, *4*, 277–283. [CrossRef]
105. Yu, H.; Liao, Q.; Kang, Z.; Wang, Z.; Liu, B.; Zhang, X.; Du, J.; Ou, Y.; Hong, M.; Xiao, J.; et al. Atomic-Thin ZnO Sheet for Visible-Blind Ultraviolet Photodetection. *Small* **2020**, *16*, e2005520. [CrossRef] [PubMed]
106. Feng, W.; Wang, X.; Zhang, J.; Wang, L.; Zheng, W.; Hu, P.; Cao, W.; Yang, B. Synthesis of two-dimensional β-Ga2O3 nanosheets for high-performance solar blind photodetectors. *J. Mater. Chem. C* **2014**, *2*, 3254–3259. [CrossRef]
107. Alsaif, M.M.Y.A.; Field, M.R.; Murdoch, B.J.; Daeneke, T.; Latham, K.; Chrimes, A.F.; Zoolfakar, A.S.; Russo, S.P.; Ou, J.Z.; Kalantar-Zadeh, K. Substoichiometric two-dimensional molybdenum oxide flakes: A plasmonic gas sensing platform. *Nanoscale* **2014**, *6*, 12780–12791. [CrossRef]
108. Han, J.W.; Rim, T.; Baek, C.K.; Meyyappan, M. Chemical Gated Field Effect Transistor by Hybrid Integration of One-Dimensional Silicon Nanowire and Two-Dimensional Tin Oxide Thin Film for Low Power Gas Sensor. *ACS Appl. Mater. Interfaces* **2015**, *7*, 21263–21269. [CrossRef] [PubMed]
109. Cao, L.; Park, J.S.; Fan, P.; Clemens, B.; Brongersma, M.L. Resonant germanium nanoantenna photodetectors. *Nano Lett.* **2010**, *10*, 1229–1233. [CrossRef]
110. Kallel, H.; Arbouet, A.; Benassayag, G.; Chehaidar, A.; Potié, A.; Salem, B.; Baron, T.; Paillard, V. Tunable enhancement of light absorption and scattering in Si 1-xGe x nanowires. *Phys. Rev. B-Condens. Matter Mater. Phys.* **2012**, *86*, 085318. [CrossRef]
111. Rinaldi, R.; Cingolani, R.; Lepore, M.; Ferrara, M.; Catalano, I.M.; Rossi, F.; Rota, L.; Molinari, E.; Lugli, P.; Marti, U.; et al. Exciton Binding Energy in GaAs V-Shaped Quantum Wires. *Phys. Rev. Lett.* **1994**, *73*, 2899–2902. [CrossRef]
112. Nehari, K.; Cavassilas, N.; Autran, J.L.; Bescond, M.; Munteanu, D.; Lannoo, M. Influence of band-structure on electron ballistic transport in silicon nanowire MOSFET's: An atomistic study. In Proceedings of the 35th European Solid-State Device Research Conference, Grenoble, France, 16 September 2005; pp. 229–232. [CrossRef]
113. Chuang, S.; Gao, Q.; Kapadia, R.; Ford, A.C.; Guo, J.; Javey, A. Ballistic InAs nanowire transistors. *Nano Lett.* **2013**, *13*, 555–558. [CrossRef]
114. Estrada Saldaña, J.C.; Niquet, Y.M.; Cleuziou, J.P.; Lee, E.J.H.; Car, D.; Plissard, S.R.; Bakkers, E.P.A.M.; De Franceschi, S. Split-Channel Ballistic Transport in an InSb Nanowire. *Nano Lett.* **2018**, *18*, 2282–2287. [CrossRef]
115. Adu, K.W.; Gutiérrez, H.R.; Kim, U.J.; Sumanasekera, G.U.; Eklund, P.C. Confined Phonons in Si Nanowires. *Nano Lett.* **2005**, *5*, 409–414. [CrossRef]
116. Ponomareva, I.; Srivastava, D.; Menon, M. Thermal conductivity in thin silicon nanowires: Phonon confinement effect. *Nano Lett.* **2007**, *7*, 1155–1159. [CrossRef] [PubMed]
117. Tambe, M.J.; Lim, S.K.; Smith, M.J.; Allard, L.F.; Gradečak, S. Realization of defect-free epitaxial core-shell GaAs/AlGaAs nanowire heterostructures. *Appl. Phys. Lett.* **2008**, *93*, 2013–2016. [CrossRef]
118. Ercolani, D.; Rossi, F.; Li, A.; Salviati, G.; Grillo, V.; Sorba, L.; Beltram, F.; Ercolani, D.; Roddaro, S.; Rossi, F. InAs/InSb nanowire heterostructures grown by chemical beam epitaxy. *Nanotechnology* **2009**, *20*, 505605. [CrossRef]
119. Pura, J.L.; Anaya, J.; Souto, J.; Prieto, A.C.; Rodríguez, A.; Rodríguez, T.; Periwal, P.; Baron, T.; Jiménez, J. Electromagnetic field enhancement effects in group IV semiconductor nanowires. A Raman spectroscopy approach. *J. Appl. Phys.* **2018**, *123*, 114302. [CrossRef]
120. Cui, Y.; Zhong, Z.; Wang, D.; Wang, W.U.; Lieber, C.M. High performance silicon nanowire field effect transistors. *Nano Lett.* **2003**, *3*, 149–152. [CrossRef]
121. Heinzig, A.; Slesazeck, S.; Kreupl, F.; Mikolajick, T.; Weber, W.M. Reconfigurable silicon nanowire transistors. *Nano Lett.* **2012**, *12*, 119–124. [CrossRef] [PubMed]
122. Garnett, E.; Yang, P. Light Trapping in Silicon Nanowire Solar Cells. *Nano Lett.* **2010**, *10*, 1082–1087. [CrossRef]
123. Otnes, G.; Borgström, M.T. Towards high efficiency nanowire solar cells. *Nano Today* **2017**, *12*, 31–45. [CrossRef]

124. Li, G.; Kwok, H.S. Silicon nanowire solar cells. In *Advances in Silicon Solar Cells*; Springer: Cham, Switzerland, 2018; pp. 269–298. [CrossRef]
125. Joyce, H.J.; Gao, Q.; Hoe Tan, H.; Jagadish, C.; Kim, Y.; Zou, J.; Smith, L.M.; Jackson, H.E.; Yarrison-Rice, J.M.; Parkinson, P.; et al. III-V semiconductor nanowires for optoelectronic device applications. *Prog. Quantum Electron.* **2011**, *35*, 23–75. [CrossRef]
126. Wallentin, J.; Anttu, N.; Asoli, D.; Huffman, M.; Åberg, I.; Magnusson, M.H.; Siefer, G.; Fuss-Kailuweit, P.; Dimroth, F.; Witzigmann, B.; et al. InP Nanowire Array Solar Cells Achieving 13.8% Efficiency by Exceeding the Ray Optics Limit. *Science* **2013**, *339*, 1057–1060. [CrossRef]
127. Aberg, I.; Vescovi, G.; Asoli, D.; Naseem, U.; Gilboy, J.P.; Sundvall, C.; Dahlgren, A.; Svensson, K.E.; Anttu, N.; Bjork, M.T.; et al. A GaAs nanowire array solar cell with 15.3% efficiency at 1 sun. *IEEE J. Photovolt.* **2016**, *6*, 185–190. [CrossRef]
128. Lind, E. High frequency III-V nanowire MOSFETs. *Semicond. Sci. Technol.* **2016**, *31*, 093005. [CrossRef]
129. Zhuang, X.; Ning, C.Z.; Pan, A. Composition and bandgap-graded semiconductor alloy nanowires. *Adv. Mater.* **2012**, *24*, 13–33. [CrossRef] [PubMed]
130. Wang, Z.L. Nanobelts, nanowires, and nanodiskettes of semiconducting oxides—From materials to nanodevices. *Adv. Mater.* **2003**, *15*, 432–436. [CrossRef]
131. Cui, J. Zinc oxide nanowires. *Mater. Charact.* **2012**, *64*, 43–52. [CrossRef]
132. Hung, C.M.; Le, D.T.T.; Van Hieu, N. On-chip growth of semiconductor metal oxide nanowires for gas sensors: A review. *J. Sci. Adv. Mater. Devices* **2017**, *2*, 263–285. [CrossRef]
133. Huang, Y.; Duan, X.; Lieber, C.M. Nanowires for integrated multicolor nanophotonics. *Small* **2005**, *1*, 142–147. [CrossRef]
134. Utama, M.I.B.; Zhang, J.; Chen, R.; Xu, X.; Li, D.; Sun, H.; Xiong, Q. Synthesis and optical properties of II-VI 1D nanostructures. *Nanoscale* **2012**, *4*, 1422–1435. [CrossRef]
135. Yao, M.; Cong, S.; Arab, S.; Huang, N.; Povinelli, M.L.; Cronin, S.B.; Dapkus, P.D.; Zhou, C. Tandem Solar Cells Using GaAs Nanowires on Si: Design, Fabrication, and Observation of Voltage Addition. *Nano Lett.* **2015**, *15*, 7217–7224. [CrossRef]
136. Yi, R.; Zhang, X.; Li, C.; Zhao, B.; Wang, J.; Li, Z.; Gan, X.; Li, L.; Li, Z.; Zhang, F.; et al. Self-frequency-conversion nanowire lasers. *Light Sci. Appl.* **2022**, *11*, 120. [CrossRef]
137. Steinhauer, S.; Brunet, E.; Maier, T.; Mutinati, G.C.; Köck, A.; Freudenberg, O.; Gspan, C.; Grogger, W.; Neuhold, A.; Resel, R. Gas sensing properties of novel CuO nanowire devices. *Sens. Actuators B Chem.* **2013**, *187*, 50–57. [CrossRef]
138. Storm, K.; Nylund, G.; Samuelson, L.; Micolich, A.P. Realizing lateral wrap-gated nanowire FETs: Controlling gate length with chemistry rather than lithography. *Nano Lett.* **2012**, *12*, 1–6. [CrossRef] [PubMed]
139. Shah, K.W.; Xiong, T. Multifunctional metallic nanowires in advanced building applications. *Materials* **2019**, *12*, 1731. [CrossRef] [PubMed]
140. Lyons, P.E.; De, S.; Elias, J.; Schamel, M.; Philippe, L.; Bellew, A.T.; Boland, J.J.; Coleman, J.N. High-performance transparent conductors from networks of gold nanowires. *J. Phys. Chem. Lett.* **2011**, *2*, 3058–3062. [CrossRef]
141. Lopez-Diaz, D.; Merino, C.; Velázquez, M.M. Modulating the optoelectronic properties of silver nanowires films: Effect of capping agent and deposition technique. *Materials* **2015**, *8*, 7622–7633. [CrossRef]
142. Jiu, J.; Suganuma, K. Metallic nanowires and their application. *IEEE Trans. Compon. Packag. Manuf. Technol.* **2016**, *6*, 1733–1751. [CrossRef]
143. Im, H.G.; Jang, J.; Jeon, Y.; Noh, J.; Jin, J.; Lee, J.Y.; Bae, B.S. Flexible Transparent Crystalline-ITO/Ag Nanowire Hybrid Electrode with High Stability for Organic Optoelectronics. *ACS Appl. Mater. Interfaces* **2020**, *12*, 56462–56469. [CrossRef]
144. Kwon, J.; Suh, Y.D.; Lee, J.; Lee, P.; Han, S.; Hong, S.; Yeo, J.; Lee, H.; Ko, S.H. Recent progress in silver nanowire based flexible/wearable optoelectronics. *J. Mater. Chem. C* **2018**, *6*, 7445–7461. [CrossRef]
145. Ditlbacher, H.; Hohenau, A.; Wagner, D.; Kreibig, U.; Rogers, M.; Hofer, F.; Aussenegg, F.R.; Krenn, J.R. Silver nanowires as surface plasmon resonators. *Phys. Rev. Lett.* **2005**, *95*, 257403. [CrossRef]
146. Kang, S.; Cho, S.; Shanker, R.; Lee, H.; Park, J.; Um, D.S.; Lee, Y.; Ko, H. Transparent and conductive nanomembranes with orthogonal silver nanowire arrays for skin-attachable loudspeakers and microphones. *Sci. Adv.* **2018**, *4*, eaas8772. [CrossRef]
147. Xu, L.; Hou, Y.; Zhang, M.; Cheng, T.; Huang, W.; Yao, C.; Wu, Q. Electrochemical sensor based on silver nanowires modified electrode for determination of cholesterol. *Anal. Methods* **2015**, *7*, 5649–5653. [CrossRef]
148. Salvo-Comino, C.; Martin-Pedrosa, F.; Garcia-Cabezon, C.; Rodriguez-Mendez, M.L. Silver nanowires as electron transfer mediators in electrochemical catechol biosensors. *Sensors* **2021**, *21*, 899. [CrossRef]
149. Salvo-Comino, C.; Martín-Bartolomé, P.; Pura, J.L.; Perez-Gonzalez, C.; Martin-Pedrosa, F.; García-Cabezón, C.; Rodríguez-Méndez, M.L. Improving the performance of a bioelectronic tongue using silver nanowires: Application to milk analysis. *Sens. Actuators B Chem.* **2022**, *364*, 131877. [CrossRef]
150. Bagal-Kestwal, D.R.; Pan, M.H.; Chiang, B.H. Electrically nanowired-enzymes for probe modification and sensor fabrication. *Biosens. Bioelectron.* **2018**, *121*, 223–235. [CrossRef]
151. Tao, A.; Kim, F.; Hess, C.; Goldberger, J.; He, R.; Sun, Y.; Xia, Y.; Yang, P. Langmuir-Blodgett silver nanowire monolayers for molecular sensing using surface-enhanced Raman spectroscopy. *Nano Lett.* **2003**, *3*, 1229–1233. [CrossRef]
152. Badr, Y.; Mahmoud, M.A. Effect of silver nanowires on the surface-enhanced Raman spectra (SERS) of the RNA bases. *Spectrochim. Acta-Part A Mol. Biomol. Spectrosc.* **2006**, *63*, 639–645. [CrossRef]
153. Yu, L.; Lu, L.; Zeng, L.; Yan, X.; Ren, X.; Wu, J.Z. Double Ag Nanowires on a Bilayer MoS2Flake for Surface-Enhanced Raman Scattering. *J. Phys. Chem. C* **2021**, *125*, 1940–1946. [CrossRef]

154. Guo, X.; Ma, Y.; Wang, Y.; Tong, L. Nanowire plasmonic waveguides, circuits and devices. *Laser Photonics Rev.* **2013**, *7*, 855–881. [CrossRef]
155. Wu, W.; Battie, Y.; Lemaire, V.; Decher, G.; Pauly, M. Structure-Dependent Chiroptical Properties of Twisted Multilayered Silver Nanowire Assemblies. *Nano Lett.* **2021**, *21*, 8298–8303. [CrossRef]
156. Keshavarz Hedayati, M.; Elbahri, M. Review of Metasurface Plasmonic Structural Color. *Plasmonics* **2017**, *12*, 1463–1479. [CrossRef]